

Article

Study on the Microscopic Mechanism of the Grain Refinement of Al-Ti-B Master Alloy

Lianfeng Yang, Huan Zhang, Xiran Zhao, Bo Liu, Xiumin Chen * and Lei Zhou *

Faculty of Metallurgical and Energy Engineering, Kunming University of Science and Technology, Kunming 650000, China

* Correspondence: chenxumin@kust.edu.cn (X.C.); zhoulei@kust.edu.cn (L.Z.)

Abstract: In the present work, the structure and properties of Ti_nB_n ($n = 2\text{--}12$) clusters were studied, and the microstructure of a Al-Ti-B system was simulated by molecular dynamics to determine the grain refinement mechanism of an Al-Ti-B master alloy in Al alloy. Based on the density functional theory method, the structural optimization and property calculations of Ti_nB_n ($n = 2\text{--}12$) clusters were carried out. The clusters at the lowest energy levels indicated that the Ti and B atoms were prone to form TiB_2 structures, and the TiB_2 structures tended to be on the surface of the clusters. The $Ti_{10}B_{10}$ cluster was determined to be the most stable structure in the range of n from 2 to 12 by average binding energy and second-order difference energy. The analysis of HOMOs and LUMOs suggested that TiB_2 was the active center in the cluster; the activity of Ti was high, but the activity of B atoms decreased as the cluster size n increased. Meanwhile, the prediction of reaction sites by Fukui function, condensed Fukui function, and condensed dual descriptor identify that Ti atoms were more active than B atoms. Furthermore, TiB_2 structures were found in the Al-Ti-B system simulated by the ab initio molecular dynamics method, and there were Al atoms growing on the Ti atoms in the TiB_2 . Based on the above analysis, this study suggests that TiB_2 may be a heterogeneous nucleation center of α -Al. This work helps to further understand the mechanism of Al-Ti-B induced heterogeneous nucleation in Al alloys, which can provide theoretical guidance for related experiments.



Citation: Yang, L.; Zhang, H.; Zhao, X.; Liu, B.; Chen, X.; Zhou, L. Study on the Microscopic Mechanism of the Grain Refinement of Al-Ti-B Master Alloy. *Metals* **2024**, *14*, 197. <https://doi.org/10.3390/met14020197>

Academic Editor: Luis Antonio Barrales-Mora

Received: 28 December 2023

Revised: 21 January 2024

Accepted: 4 February 2024

Published: 5 February 2024



Copyright: © 2024 by the authors. Licensee MDPI, Basel, Switzerland. This article is an open access article distributed under the terms and conditions of the Creative Commons Attribution (CC BY) license (<https://creativecommons.org/licenses/by/4.0/>).

Keywords: heterogeneous nucleation; TiB_2 ; grain refinement; Ti_nB_n clusters

1. Introduction

Al alloys are increasingly being used in the automotive field to meet the demands for lower fuel consumption and emissions. As a result of their widespread use, requirements for performance are also increasing. During the solidification process of alloys, coarse columnar crystals may form, resulting in a large number of defects that affect the quality and performance of the casting. A large number of studies have concentrated on methods of reducing grain size, such as optimizing the casting process of alloys, electromagnetic or ultrasonic vibration, and the addition of grain refiners. The most popular method for microstructure modification is to add refining agents in the preparation process of alloy materials. This method is simple and controllable, low cost, and does not require the assistance of complex equipment. Therefore, grain refinement is an important method to improve the quality of Al alloys. It can increase the nucleation center, reduce the size of α -Al grains, and inhibit the generation of columnar crystals during the cooling crystallization process. The improvement in mechanical properties is largely due to the evolution of the microstructure. Fine grain size can reduce the microporosity and size of second phase particles, reduce the casting defects so as to improve the mechanical properties [1–4].

Al-Ti-B master alloy is one of the most popular grain refiners used in the production of industrial Al alloys; it provides excellent grain refinement performance in continuous and semi-continuous casting of forged alloys. According to reports in the literature, TiB_2 and $TiAl_3$ are the main phases of Al-Ti-B grain refiners [5,6]. Some scholars believe that TiB_2

particles alone do not have a grain refining effect on Al alloys. Only by forming a TiAl_3 thin layer on the surface can they activate it to become an effective nucleation centre for α -Al [7–10]. However, Wang's study [11] found that the distance between Al atoms on the Ti-terminated surface of TiB_2 is similar to the distance found in Al_3Ti , so the thin layer of TiB_2 surface observed in the experiment may be strained Al on the Ti-terminated surface. Meanwhile, Al_3Ti particles have high solubility in the melt and can be completely dissolved in a short period of time, so they are unlikely to become a heterogeneous nucleation point of α -Al [12]. Jones [13,14] summarized that TiB_2 introduces multiple heterogeneous nucleation sites, and dendritic α -Al becomes a fine equiaxed grain structure; it can also improve the morphology of eutectic Si from large flake to particles [15–18]. TiB_2 has a good grain refinement effect on α -Al.

Li et al. [19] found experimentally that the addition of TiB_2 in A390 alloy reduced the average grain size of α -Al and eutectic Si, and significantly improved the ductility and mechanical properties of the material. Greer et al. [20] found by model predictions that the heterogeneous nucleus of TiB_2 particles in Al-Ti-B refiners occurs at a lower degree of undercooling. In a recent study, Feng et al. [21] investigated the non-homogeneous nucleus and growth kinetics of Al on a (0001) TiB_2 surface; they concluded that TiB_2 particles can act as nucleating agents for Al, and that α -Al grows directly on the (0001) TiB_2 surface. David [22] compared several possible nucleation mechanisms of TiB_2 terminated with Ti, TiB_2 terminated with B, and TiB_2 covered with TiAl_3 by DFT simulation, and obtained the results that TiB_2 terminated with Ti was more stable than with B, and that direct nucleation of α -Al at the Ti-terminated TiB_2 was a more favorable nucleation mechanism than the formation of a TiAl_3 thin layer. Liu et al. [23] investigated the effect of Al-Ti-B intermediate alloy, and La on W319 alloy, and found that Al-Ti-B significantly reduced the secondary dendrite arm spacing of the alloy, improved the hardness, and decreased the number of micropores. To a certain extent, the influence of defects produced in the casting process on the properties of the alloy was reduced. Knaislová's group [24] characterised the microstructure of AlSi7Mg0.3 alloys with the addition of Al-Ti-B refiners; compared with the test results, it was found that the grain size of Al was significantly reduced, and the irregular eutectic Si phase was transformed into round or short rod. In studies of Sun et al. [25–29], the number and size of columnar crystals in Al alloys materials significantly decreased with the addition of TiB_2 particles, while the tensile strength and ductility of the materials were improved.

The actual production of alloy materials generally involves a process from liquid to solid, but many phenomena are difficult to observe. Changes of microstructure in the alloy melt during solidification have an important influence on the properties of the material; now computer simulation can be used to understand the nature of microstructure evolution. Simulations are being widely used in the study of alloy materials. By calculating the structure and properties of clusters, it is possible to speculate the changes in the microstructure of the alloy and possible reactions between the components, as well as to understand the geometric structure and interaction of the molecules. At present, cluster simulation is widely discussed in catalysis [30–32], hydrogen storage [33], alloy materials [34], and other fields. In addition, ab initio molecular dynamics simulation is helpful to observe the trajectories of atoms in the alloys, and predict possible results. The electron transfer and bonding of the components can also be analysed by electronic structure calculations. The microstructure of the Al-Ti-B system was analyzed by simulation in this study.

The process of grain refinement in Al-Ti-B grain refiner is still controversial. So far, the study of grain refinement in Al-Ti-B intermediate alloys has been conducted mostly by experimental methods. Observing nucleation behaviour during the early stages of solidification through experimental methods is challenging due to its occurrence at high temperature, microscopic scale, and for very short periods of time; common experimental means do not provide a good indication of changes in the structure of the alloy melt during the cooling process. The evolution of molecules in melts is crucial. Ti_nB_n ($n = 2–12$) clusters were studied, at the same time, Al-Ti-B system simulation was conducted to understand

the possible behavior of Ti and B in this paper. The grain refinement behaviour of Ti and B atoms in Al alloys was investigated by calculating the molecular structure changes and electronic properties of Ti_nB_n clusters and the Al-Ti-B system. This study is significant in exploring the refining mechanism of Al-Ti-B grain refiners.

2. Computational Details

2.1. Calculation of Clusters

Firstly, the primary structures of the Ti_nB_n ($n = 2\text{--}12$) clusters were built and optimized in Materials Studio [35]. The optimization conditions were: DND (double numerical plus d-functions) basis set, and gradient-corrected functionals in the form of generalized gradient approximation (GGA) with the Perdew–Burke–Ernzerhof (PBE) [36] functional; the energy and gradient convergence accuracy were 10^{-5} Hartree and 0.004 \AA ; and maximum displacement was 0.3 \AA . Secondly, in order to obtain a more comprehensive cluster structure, the lowest energy structure was searched by ab initio molecular dynamics, and the NVT [37] ensemble, the DNP (double numerical plus polarization) basis set, and GGA-PBE exchange correlation function were used; temperature was set to 500 K, the time step was 1 fs and ran for a total of 100 ps. Finally, the cluster structure was reoptimized using Gaussian16 [38], and the energy was calculated on the level of M06L [39] /6-311G (d, p).

The stability of the clusters was calculated using Gaussian16. The Multiwfn program [40–42] was used to calculate the condensed Fukui function and condensed dual descriptor of the $Ti_{10}B_{10}$ cluster. On the basis of the output file of the Multiwfn program, the HOMOs (Highest Occupied Molecular Orbital); LUMOs (Lowest Unoccupied Molecular Orbital) of all clusters; and the Fukui function images were plotted using VMD193 [43] software, and the electronic isosurface of the $Ti_{10}B_{10}$ cluster colored by Fukui function was drawn using GaussView6.0 [44].

2.2. Ab Initio Molecular Dynamics Calculation (AIMD)

Ab initio molecular dynamics simulations of the Al-Ti-B system were carried out using the VASP [45] package and the SCAN [46] Meta-GGA functional (Strongly Constrained and Appropriately Normed Semilocal Density functional) and the NVT ensemble. K mesh was set at $1 \times 1 \times 1$, energy cut was 400 eV, and the convergence standard for energy was 10^{-6} eV/atom. The simulation temperature was 698 K. The simulation time was 10 ps (picosecond) with a time step of 1 fs (femtosecond). The lattice parameter was $a = 16.0466 \text{ \AA}$; $b = 16.08830 \text{ \AA}$; $c = 15.9796016 \text{ \AA}$; $\alpha = 90.1209^\circ$; $\beta = 90.0634^\circ$; $\gamma = 90.2491^\circ$, and there were 199 Al; 6 Ti; and 6 B atoms in the supercell.

3. Results and Discussion

3.1. The Ground State Structures of Ti_nB_n ($n = 2\text{--}12$) Clusters

The lowest energy structures of Ti_nB_n ($n = 2\text{--}12$) clusters are shown in Table 1, and all of them have point group symmetry structures of C1, so the symmetry of the clusters is poor. On the whole, Ti atoms are distributed outside the clusters, B atoms are relatively concentrated, and they are gradually surrounded by Ti atoms with the number of atoms increasing. Analysing the structures of the clusters revealed that Ti and B formed TiB_2 structures. As the cluster size increased, the number of TiB_2 structures increased and they were connected by a shared B/Al atom. Therefore, Ti_nB_n ($n = 2\text{--}12$) clusters can be considered to be composed of multiple TiB_2 structures. In addition, atomic arrangement was a major factor influencing growth behaviour [47]. As can be seen from Table 1, TiB_2 tended to be distributed on the surface of the clusters, with the B atoms towards the interior of the clusters, and the Ti atoms towards the surface of the clusters. It has been reported [22] that the Ti termination layer of TiB_2 is more stable to contact with Al melt than the B termination layer of TiB_2 .

Table 1. Ground state structures of Ti_nB_n ($n = 2-12$) clusters.

3.2. Stability of Ti_nB_n ($n = 2\text{--}12$) Clusters

The stability of the clusters can be assessed by the average binding energy (E_b) and the second-order difference energy ($\Delta_2 E$), which are calculated by the following formulas:

$$E_b = [nE(Ti) + nE(B) - E(Ti_nB_n)]/(2n) \quad (1)$$

$$\Delta_2 E = E(T_{n+1}B_{n+1}) + E(T_{n-1}B_{n-1}) - 2E(T_nB_n) \quad (2)$$

$E(Ti)$, $E(B)$, $E(Ti_{n+1}B_{n+1})$, $E(Ti_{n-1}B_{n-1})$ and $E(Ti_nB_n)$ denote the energy of Ti atoms, B atoms, $Ti_{n+1}B_{n+1}$, $Ti_{n-1}B_{n-1}$ and Ti_nB_n clusters, respectively.

If the binding energy is large, it means that the cluster configuration is stable. Figure 1 shows the curve of the average binding energy with the change of n . As can be seen, it gradually increased with the increase of the number of atoms, indicating that the interatomic interaction was enhanced and the clusters became more and more stable. Furthermore, the average binding energy reached a maximum at $n = 10$, which indicates that the $\text{Ti}_{10}\text{B}_{10}$ cluster is the most stable.

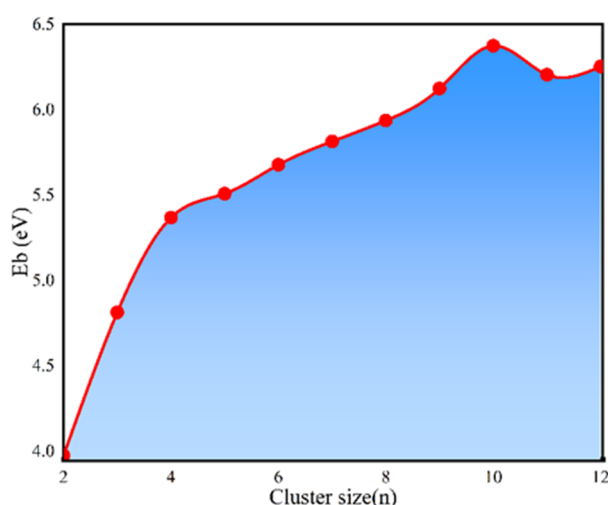


Figure 1. Average binding energy of Ti_nB_n ($n = 2-12$) clusters.

The second-order difference energy can reflect the stability of the clusters. The larger it is, the better the cluster stability. From Figure 2, it is easy to see when $n \leq 7$, the stability of clusters with an even number of n was higher than that with an odd number. Otherwise, when $n = 2, 4$ and 10 , the second-order difference energy was positive, and much larger than other clusters; it was apparent that the stability of clusters Ti_2B_2 , Ti_4B_4 , and $\text{Ti}_{10}\text{B}_{10}$ was higher. In addition, as seen in Figure 2, the maximum value was achieved at $n = 10$; combined with the average binding energy, it can be considered that the $\text{Ti}_{10}\text{B}_{10}$ cluster is the most stable structure ($n = 2\text{--}12$).

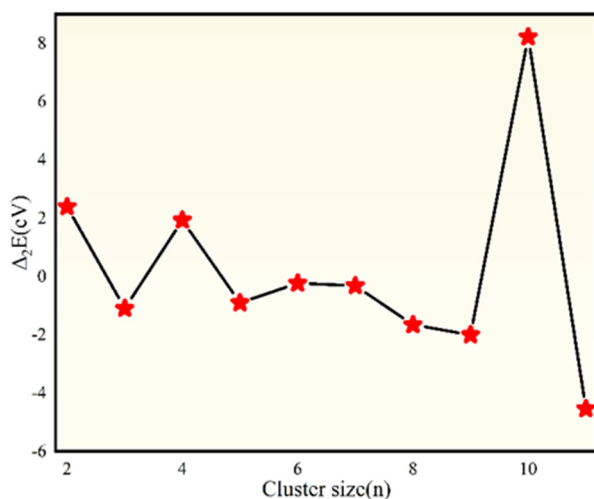


Figure 2. Second-order difference energy of Ti_nB_n ($n = 2\text{--}12$) clusters.

3.3. Prediction of Reaction Sites in Ti_nB_n ($n = 2\text{--}12$) Clusters

The properties of alloys are closely related to the electronic structure, so the HOMOs and LUMOs of Ti_nB_n ($n = 2\text{--}12$) clusters were calculated, as shown in Table 2. They are helpful to analyze the chemical reactivity of molecules. When $n = 2$, it showed that there were HOMOs and LUMOs on the surface of both Ti and B atoms, and with the gradual increase of n , there was a transfer from B atoms to Ti atoms, which were mainly distributed on the surface of Ti atoms in the TiB_2 structures. This suggested that the TiB_2 structures in the Ti_nB_n clusters were the active region of the cluster, where the activity of Ti atoms was higher than that of B atoms, and the activity of B atoms was gradually decreasing. Zhang et al. [48] reported that there is a strong 3d(Ti)-3p(Al) hybridization between the Ti-terminated interface and α -Al, that is stronger than the Al-B atom bonding; α -Al is more prone to epitaxial growth on the Ti termination surface, whereas the bonding between B-terminated and Al is weak, which cannot induce the continuous growth of Al atoms. Therefore, it is hypothesized that the Ti atom in the TiB_2 structure is the attachment site for α -Al.

Table 2. HOMOs and LUMOs of Ti_nB_n ($n = 2\text{--}12$) clusters.

Categories	Ground State Structures of Ti_nB_n ($n = 2\text{--}12$) Clusters			
HOMO				

Table 2. Cont.

Categories	Ground State Structures of Ti_nB_n ($n = 2\text{--}12$) Clusters			
LUMO				
n	2	3	4	5
HOMO				
LUMO				
n	6	7	8	9
HOMO				
LUMO				
n	10	11	12	

According to the average binding energy and the second-order differential energy, $Ti_{10}B_{10}$ is the most stable structure in Ti_nB_n ($n = 2\text{--}12$). Therefore, the $Ti_{10}B_{10}$ cluster was taken as an example to predict the reaction sites in clusters by means of the Fukui function, condensed Fukui function (CFF), and condensed dual descriptor [49–51]. The electrophilic/nucleophilic reaction formula of the Fukui function [52] are approximated as follows:

$$\text{electrophilic reaction : } f^-(r) = \rho_N(r) - \rho_{N-1}(r) \quad (3)$$

$$\text{nucleophilic reaction : } f^+(r) = \rho_{N+1}(r) - \rho_N(r) \quad (4)$$

The electron density ρ_N , ρ_{N+1} and ρ_{N-1} is represented separately when the system contains N electrons, $N + 1$ electrons, and $N - 1$ electrons. The change of electron density at each position is represented by $f^-(r)$ and $f^+(r)$ due to electron transfer when electrophilic or nucleophilic reaction occurs, respectively.

In Figure 3, (a) and (b) are electron isosurface maps of the Fukui function coloring for electrophilic and nucleophilic reaction predictions, respectively. Blue and red respectively represent positive and negative regions. The darker the blue regions, the larger the function value corresponding to it, and the stronger the reaction activity [53,54]. It is worth noting that the prediction of electrophilic reactions showed that the isosurface of the Fukui function mainly covered the surface of Ti atoms in Figure 3, indicating that the electrophilic reaction

is prone to occur on Ti atoms. The isosurface map of the nucleophilic reaction was consistent with the electrophilic reaction, suggesting that the nucleophilic reaction also easily occurs on the Ti atoms. As a consequence, both electrophilic and nucleophilic reactions tend to take place on Ti atoms.

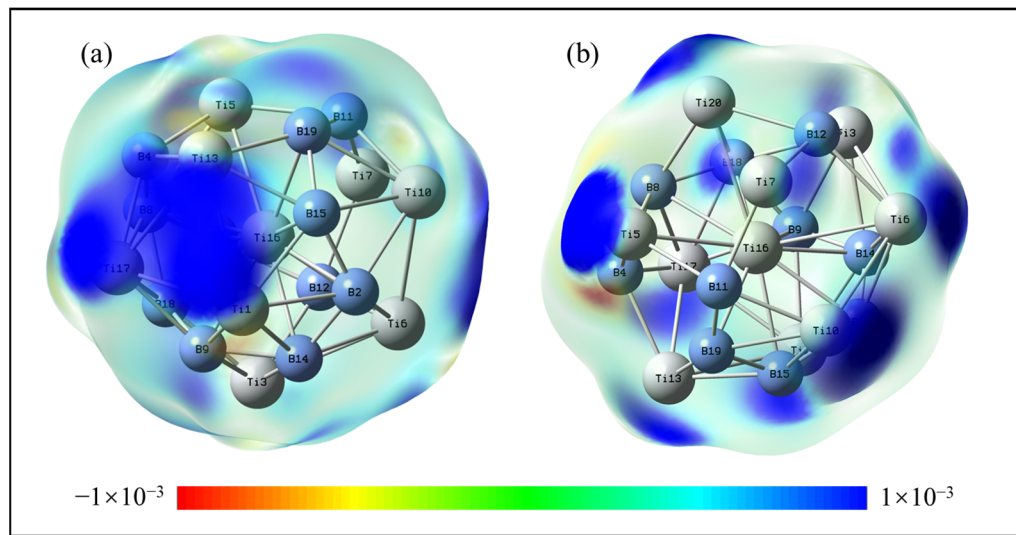


Figure 3. Fukui function isosurface maps of $\text{Ti}_{10}\text{B}_{10}$ cluster; (a) prediction of electrophilic reactions; (b) prediction of nucleophilic reactions (isovalue = 0.01a.u.).

The condensed Fukui function contracts the Fukui function to each atom to obtain their corresponding values to quantify their reactivity [55,56]. The reasonableness of the condensed Fukui function based on Hirschfeld atomic charge calculations for predicting reaction sites has been tested [52]. The values of the condensed Fukui function are listed in Figure 4.

$$\text{electrophilic reaction : } f_A^- = q_{N-1}^A - q_N^A \quad (5)$$

$$\text{nucleophilic reaction : } f_A^+ = q_N^A - q_{N+1}^A \quad (6)$$

where q_{N-1}^A , q_N^A , q_{N+1}^A represent the charges of atom A in the system with $N - 1$, N , $N + 1$ electrons, and f_A^- and f_A^+ denote the condensed Fukui function corresponding to electrophilic and nucleophilic reactions, respectively.

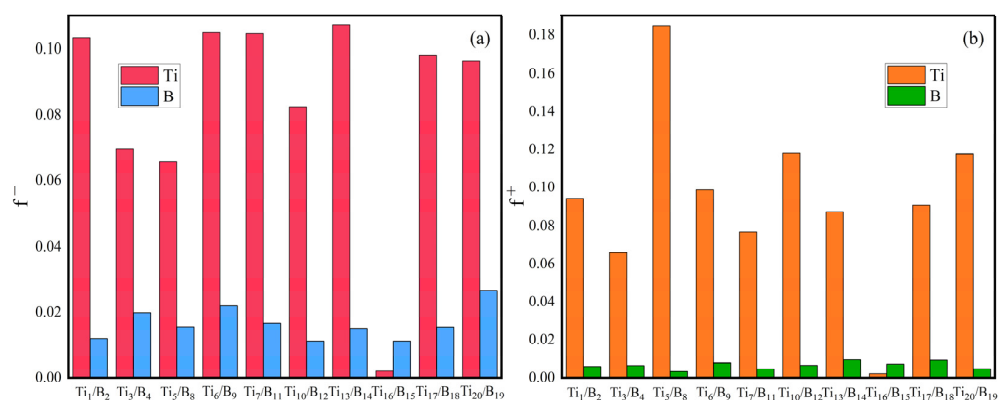


Figure 4. Condensed Fukui functions of $\text{Ti}_{10}\text{B}_{10}$ cluster; (a) f^- , red corresponds to Ti atoms, blue corresponds to B atoms; (b) f^+ , orange corresponds to Ti atoms, green corresponds to B atoms.

The size of this descriptor can reflect the degree of electrophilicity or nucleophilicity. The condensed Fukui function allows for a more intuitive comparison of the activity of atoms [57]. It can be seen from Figure 4 that in the prediction of electrophilic reaction,

the condensed Fukui function value of Ti atoms was significantly greater than that of B atoms, only the value of Ti₁₆ atoms was small, so Ti atoms were vulnerable to electrophilic attack. For the nucleophilic prediction, the condensed Fukui function values for Ti atoms were similarly much larger than those for B atoms (except for Ti₁₆ atoms), suggesting that Ti atoms were more likely to attract nucleophilic reagents. The above shows that the reactivity of Ti atoms is higher than that of B atoms; both electrophilic and nucleophilic reactions occur preferentially on Ti atoms. Han [58] et al. also concluded by first principles calculations that the adhesion at the Ti-termination interface is greater than that at the B-termination interface.

The condensed dual descriptor (CDD) is a parameter that defines the nature of the local position in a molecule as electrophilic (positive) or nucleophilic (negative) [59,60]. It is approximated as the second-order derivative of the electron density relative to the number of electrons under a fixed external potential [61]. In this article, the condensed dual descriptor of a Ti₁₀B₁₀ cluster was calculated to facilitate comparisons of the electrophilic/nucleophilic reactivity of each atom. The formula was as follows:

$$f_A^{(2)}(r) = f_A^+(r) - f_A^-(r) \quad (7)$$

The greater the negative value of CDD, the more likely it is to be the electrophilic site; the higher the positive value, the more vulnerable to nuclear attack [62]. The data in Figure 5 show that the Ti atoms had both positive and negative condensed dual descriptors, so it is possible that the Ti atoms were electrophilic or nucleophilic sites. The condensed dual descriptors of the B atoms were all negative, favoring nucleophilic reactions. However, as the maximum and minimum values of the CDD were at the Ti atoms, it can be concluded that the Ti atoms are highly reactive; as mentioned previously, Ti atoms may be the reactive site in clusters.

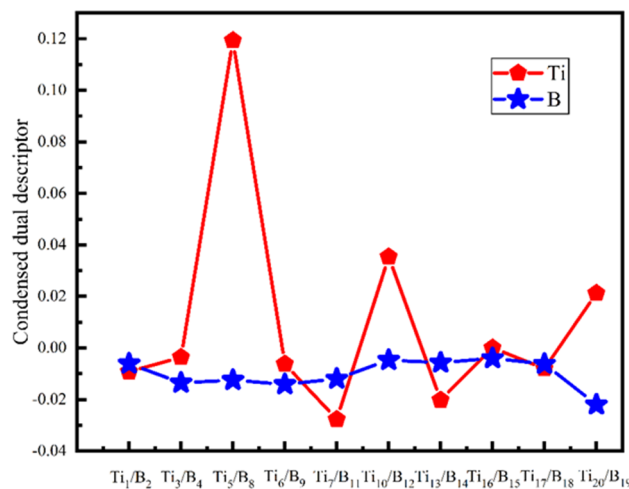


Figure 5. Condensed dual descriptor of Ti₁₀B₁₀ cluster.

3.4. Ab Initio Molecular Dynamics Simulation Results

In order to verify the structure and interaction of Ti and B atoms in Al-Ti-B alloys, in this paper, the kinetic behaviour of atoms in the Al-Ti-B system was investigated by ab initio molecular dynamics simulations. As shown in Figure 6, the variation of melt structure in the 698K system was analysed. Figure 6a shows the structure of the Al-Ti-B system before the dynamic simulation, and it can be seen that the three elements were uniformly distributed. After ab initio molecular dynamics simulation, Ti and B atoms formed the triangular structure of TiB₂. Figure 6b shows the TiB₂ structure in the system at 7000 fs, 7005 fs, 7229 fs, and 7230 fs. After ab initio molecular dynamics simulations, the TiB₂ structure was observed at 7000 fs, and there was one Al atom bonded to the Ti atom in TiB₂. Moreover, at 7005 fs, there were two Al atoms bonded to Ti in TiB₂. Then, the

epitaxial growth of Al atoms was observed at 7229 fs and 7230 fs. Zhang et al. have reported in the literature [48,63] that Al growth on the Ti-termination surface of the TiB_2 layer is then further stacked and extended. In summary, the results of the AIMD simulations are consistent with the cluster results discussed above.

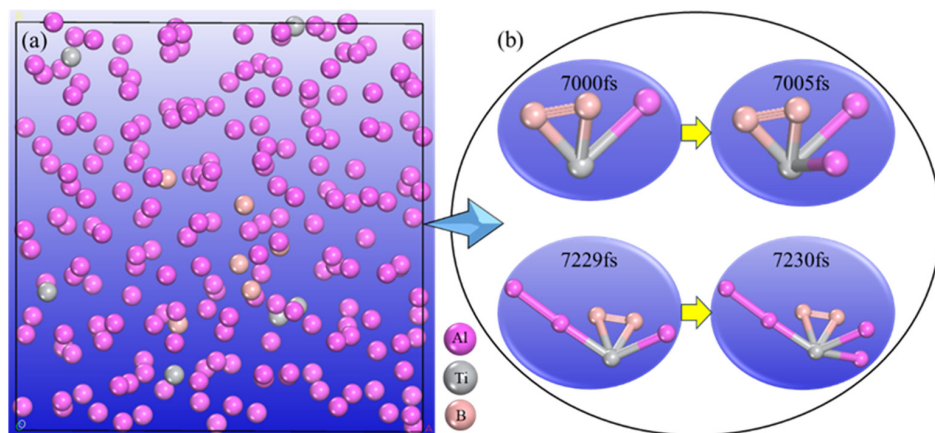


Figure 6. Structure of Al-Ti-B melt; **(a)** structure before dynamic simulation; **(b)** local structures after dynamics simulation.

In order to understand the reasons for the formation of the TiB_2 structure in the Al-Ti-B system, the electronic structure of the melt at 7000 fs was analyzed. Figure 7a shows the structure of the Al-Ti-B system. Figure 7b is an electron density difference isosurface map of TiB_2 ; the value of the isosurface was 0.06. According to the electron density, it can be seen that electrons were shared between the B atoms; B–B was a strongly covalent bond. There were shared electrons between Ti and B atoms, but the electrons were biased towards B atoms. The electron density difference section of the TiB_2 structure is shown in Figure 7c, and the location of the section is marked with a red dashed line in Figure 7a. The electron transfer between atoms is analyzed by the section diagram. In Figure 7c, blue indicates an increase in electron density, while red indicates a decrease. As can be seen, the charge density of Ti atoms decreased (red), and that of B atoms increased (blue); there were electrons transfers from Ti to B atoms. Therefore, combined with Figure 7b, Ti and B atoms were bonded in the form of ionic covalent bonds. In summary, after first-principles molecular dynamics simulation, Ti and B can generate an *in situ* TiB_2 structure; a heterogeneous nucleation center of Al atoms.

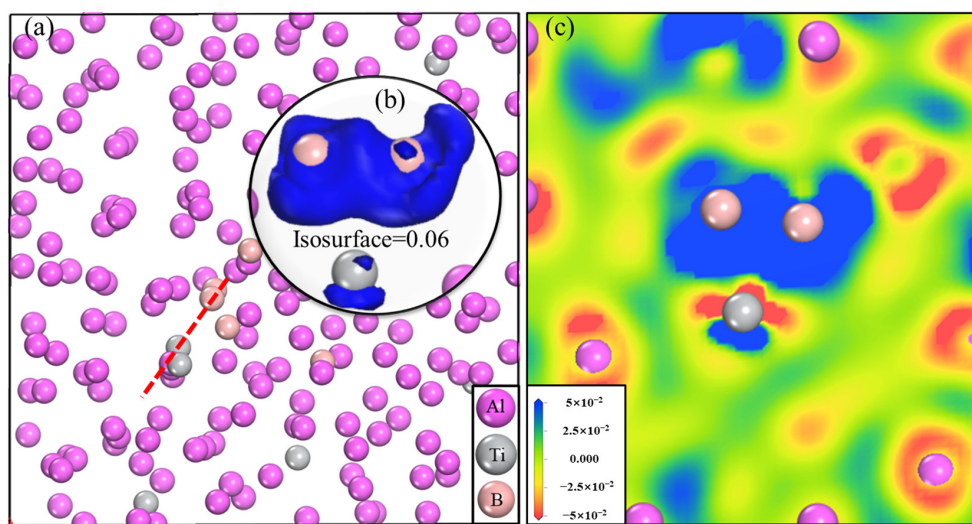


Figure 7. Electron density difference maps; **(a)** Al-Ti-B system; **(b)** electron density difference isosurface; **(c)** electron density difference section.

4. Conclusions

In this paper, Ti_nB_n ($n = 2\text{--}12$) clusters and Al-Ti-B systems were calculated. The possibility of TiB_2 as a heterogeneous nucleation centre of α -Al was discussed by analyzing structural changes and electronic properties. The following are the main conclusions:

- (1) TiB_2 triangular structures are present in the cluster structures from n equal to 2 to 12; the amount of TiB_2 increases as the cluster size increases and Ti atoms are oriented towards the surface of clusters. The average binding energy and second-order difference energy of the clusters show that the stability of the clusters increases with the increasing number of atoms, and the most stable structure is obtained at $n = 10$.
- (2) It shows that HOMOs and LUMOs are concentrated on Ti atoms within the TiB_2 structure, indicating that the TiB_2 structure is the more active part of the clusters, and the activity of Ti atoms is higher than that of B atoms. The map of Fukui function shows that the Ti atoms are more reactive than B atoms. The value of the condensed Fukui function and condensed dual descriptor suggests that the value of most Ti atoms is much larger than that of B atoms. Therefore, Ti atoms have higher reactivity.
- (3) The AIMD simulation results of the Al-Ti-B system show that Ti and B atoms can form TiB_2 structure in situ, and there are Al atoms adsorbing and growing on the Ti surface in the TiB_2 structure. The electronic structure of TiB_2 was analysed by charge density difference. The results show that B atoms are connected by strong covalent bonds, and Ti and B atoms form ionic covalent bonds.

Author Contributions: L.Y.: Conceptualization, Methodology, Software, Investigation, Writing—original draft; X.C.: Resources, Formal analysis, Software, Writing—review and editing; L.Z.: Resources, Validation, Formal analysis, Software, Writing—review and editing; H.Z.: Formal analysis, Validation; X.Z.: Formal analysis, Visualization; B.L.: Formal analysis, Validation. All authors have read and agreed to the published version of the manuscript.

Funding: This work was supported by the major science and technology special program of Yunnan Province (Grant 202102AB080004).

Data Availability Statement: The original contributions presented in the study are included in the article, further inquiries can be directed to the corresponding authors.

Conflicts of Interest: The authors declare no conflicts of interest.

References

1. Kori, S.; Murty, B.; Chakraborty, M. Development of an efficient grain refiner for Al-7Si alloy and its modification with strontium. *Mater. Sci. Eng. A* **2000**, *283*, 94–104. [[CrossRef](#)]
2. Wang, F.; Liu, Z.; Qiu, D.; Taylor, J.A.; Easton, M.A.; Zhang, M.-X. Revisiting the role of peritectics in grain refinement of Al alloys. *Acta Mater.* **2013**, *61*, 360–370. [[CrossRef](#)]
3. Quested, T. Understanding mechanisms of grain refinement of aluminium alloys by inoculation. *Mater. Sci. Technol.* **2004**, *20*, 1357–1369. [[CrossRef](#)]
4. Fan, Z.; Gao, F.; Wang, Y.; Men, H.; Zhou, L. Effect of solutes on grain refinement. *Prog. Mater. Sci.* **2022**, *123*, 100809. [[CrossRef](#)]
5. Ding, W.; Zhao, X.; Chen, T.; Zhang, H.; Liu, X.; Cheng, Y.; Lei, D. Effect of rare earth Y and Al-Ti-B master alloy on the microstructure and mechanical properties of 6063 aluminum alloy. *J. Alloys Compd.* **2020**, *830*, 154685. [[CrossRef](#)]
6. Murty, B.; Kori, S.; Chakraborty, M. Grain refinement of aluminium and its alloys by heterogeneous nucleation and alloying. *Int. Mater. Rev.* **2002**, *47*, 3–29. [[CrossRef](#)]
7. Fan, Z.; Wang, Y.; Zhang, Y.; Qin, T.; Zhou, X.; Thompson, G.; Pennycook, T.; Hashimoto, T. Grain refining mechanism in the Al/Al-Ti-B system. *Acta Mater.* **2015**, *84*, 292–304. [[CrossRef](#)]
8. Huang, B.; Liu, Y.; Zhou, Z.; Cheng, W.; Liu, X. Selective laser melting of 7075 aluminum alloy inoculated by Al-Ti-B: Grain refinement and superior mechanical properties. *Vacuum* **2022**, *200*, 111030. [[CrossRef](#)]
9. Greer, A.L. Overview: Application of heterogeneous nucleation in grain-refining of metals. *J. Chem. Phys.* **2016**, *145*, 211704. [[CrossRef](#)]
10. Mohanty, P.; Grzuleski, J. Grain refinement mechanisms of hypoeutectic Al Si alloys. *Acta Mater.* **1996**, *44*, 3749–3760. [[CrossRef](#)]
11. Wang, J.; Horsfield, A.; Schwingenschlögl, U.; Lee, P.D. Heterogeneous nucleation of solid Al from the melt by TiB_2 and Al_3Ti : An ab initio molecular dynamics study. *Phys. Rev. B* **2010**, *82*, 184203. [[CrossRef](#)]

12. Yu, F.; Liu, Z.; Zhao, R.; Yang, J.; Qiao, J.; Hu, W. Effect of Al-Ti-B master alloy on microstructure and properties of aluminum-air battery anode materials. *J. Mater. Res. Technol.* **2023**, *27*, 4908–4919. [[CrossRef](#)]
13. Jones, G.P.; Pearson, J. Factors affecting the grain-refinement of aluminum using titanium and boron additives. *Metall. Trans. B* **1976**, *7*, 223–234. [[CrossRef](#)]
14. Sigworth, G.K.; Kuhn, T.A. Grain refinement of aluminum casting alloys. *Int. J. Met.* **2007**, *1*, 31–40. [[CrossRef](#)]
15. Han, Y.; Liu, X.; Bian, X. In situ TiB₂ particulate reinforced near eutectic Al-Si alloy composites. *Compos. Part A Appl. Sci. Manuf.* **2002**, *33*, 439–444. [[CrossRef](#)]
16. Kumar, S.; Chakraborty, M.; Sarma, V.S.; Murty, B.S. Tensile and wear behaviour of in situ Al-7Si/TiB₂ particulate composites. *Wear* **2008**, *265*, 134–142. [[CrossRef](#)]
17. MAKbari, K.; Baharvandi, H.; Shirvanimoghaddam, K. Tensile and fracture behavior of nano/micro TiB₂ particle reinforced casting A356 aluminum alloy composites. *Mater. Des.* **2015**, *66*, 150–161.
18. Dong, B.-X.; Li, Q.; Wang, Z.-F.; Liu, T.-S.; Yang, H.-Y.; Shu, S.-L.; Chen, L.-Y.; Qiu, F.; Jiang, Q.-C.; Zhang, L.-C. Enhancing strength-ductility synergy and mechanisms of Al-based composites by size-tunable in-situ TiB₂ particles with specific spatial distribution. *Compos. Part B Eng.* **2021**, *217*, 108912. [[CrossRef](#)]
19. Li, P.; Li, Y.; Wu, Y.; Ma, G.; Liu, X. Distribution of TiB₂ particles and its effect on the mechanical properties of A390 alloy. *Mater. Sci. Eng. A* **2012**, *546*, 146–152. [[CrossRef](#)]
20. Greer, A.; Bunn, A.; Tronche, A.; Evans, P.; Bristow, D. Modelling of inoculation of metallic melts: Application to grain refinement of aluminium by Al-Ti-B. *Acta Mater.* **2000**, *48*, 2823–2835. [[CrossRef](#)]
21. Feng, J.; Han, Y.; Han, X.; Wang, X.; Song, S.; Sun, B.; Chen, M.; Liu, P. Atomic insights into heterogeneous nucleation and growth kinetics of Al on TiB₂ particles in undercooled Al-5Ti-1B melt. *J. Mater. Sci. Technol.* **2023**, *156*, 72–82. [[CrossRef](#)]
22. Wearing, D.; Horsfield, A.P.; Xu, W.; Lee, P.D. Which wets TiB₂ inoculant particles: Al or Al₃Ti? *J. Alloys Compd.* **2016**, *664*, 460–468. [[CrossRef](#)]
23. Liu, X.; Wang, B.; Li, Q.; Wang, J.; Zhang, C.; Xue, C.; Yang, X.; Tian, G.; Liu, X.; Tang, H. Quantifying the effects of grain refiners Al-Ti-B and La on the microstructure and mechanical properties of W319 alloy. *Metals* **2022**, *12*, 627. [[CrossRef](#)]
24. Knaislová, A.; Michna, Š.; Hren, I.; Vlach, T.; Michalcová, A.; Novák, P.; Stančeková, D. Microstructural characteristics of Al-Ti-B inoculation wires and their addition to the AlSi7Mg0.3 alloy. *Materials* **2022**, *15*, 7626. [[CrossRef](#)] [[PubMed](#)]
25. Sun, T.; Wang, H.; Gao, Z.; Wu, Y.; Wang, M.; Jin, X.; Leung, C.L.A.; Lee, P.; Fu, Y.; Wang, H. The role of in-situ nano-TiB₂ particles in improving the printability of noncastable 2024Al alloy. *Mater. Res. Lett.* **2022**, *10*, 656–665. [[CrossRef](#)]
26. Youssef, Y.; Dashwood, R.; Lee, P. Effect of clustering on particle pushing and solidification behaviour in TiB₂ reinforced aluminium PMMCs. *Compos. Part A Appl. Sci. Manuf.* **2005**, *36*, 747–763. [[CrossRef](#)]
27. Wang, M.; Chen, D.; Chen, Z.; Wu, Y.; Wang, F.; Ma, N.; Wang, H. Mechanical properties of in-situ TiB₂/A356 composites. *Mater. Sci. Eng. A* **2014**, *590*, 246–254. [[CrossRef](#)]
28. Xi, L.; Gu, D.; Guo, S.; Wang, R.; Ding, K.; Prashanth, K.G. Grain refinement in laser manufactured Al-based composites with TiB₂ ceramic. *J. Mater. Res. Technol.* **2020**, *9*, 2611–2622. [[CrossRef](#)]
29. Xiao, Y.; Bian, Z.; Wu, Y.; Ji, G.; Li, Y.; Li, M.; Lian, Q.; Chen, Z.; Addad, A.; Wang, H. Effect of nano-TiB₂ particles on the anisotropy in an AlSi10Mg alloy processed by selective laser melting. *J. Alloys Compd.* **2019**, *798*, 644–655. [[CrossRef](#)]
30. Guo, X.; Li, X.; Li, Y.; Yang, J.; Wan, X.; Chen, L.; Liu, J.; Liu, X.; Yu, R.; Zheng, L. Molecule template method for precise synthesis of Mo-based alloy clusters and electrocatalytic nitrogen reduction on partially reduced PtMo alloy oxide cluster. *Nano Energy* **2020**, *78*, 105211. [[CrossRef](#)]
31. Kurashige, W.; Hayashi, R.; Wakamatsu, K.; Kataoka, Y.; Hossain, S.; Iwase, A.; Kudo, A.; Yamazoe, S.; Negishi, Y. Atomic-level understanding of the effect of heteroatom doping of the cocatalyst on water-splitting activity in AuPd or AuPt alloy cluster-loaded BaLa₄Ti₄O₁₅. *ACS Appl. Energy Mater.* **2019**, *2*, 4175–4187. [[CrossRef](#)]
32. Rodriguez-Kessler, P.; Muñoz-Castro, A.; Alonso-Dávila, P.; Aguilera-Granja, F.; Rodríguez-Domínguez, A. Structural, electronic and catalytic properties of bimetallic PtnAgn ($n = 1\text{--}7$) clusters. *J. Alloys Compd.* **2020**, *845*, 155897. [[CrossRef](#)]
33. Huang, H.; Wu, B.; Gao, Q.; Li, P.; Yang, X. Structural, electronic and spectral properties referring to hydrogen storage capacity in binary alloy ScBn ($n = 1\text{--}12$) clusters. *Int. J. Hydrogen Energy* **2017**, *42*, 21086–21095. [[CrossRef](#)]
34. Liu, Q.; Cheng, L. Structural evolution and electronic properties of Cu-Zn alloy clusters. *J. Alloys Compd.* **2019**, *771*, 762–768. [[CrossRef](#)]
35. Delley, B. An all-electron numerical method for solving the local density functional for polyatomic molecules. *J. Chem. Phys.* **1990**, *92*, 508–517. [[CrossRef](#)]
36. Perdew, J.P.; Burke, K.; Ernzerhof, M. Generalized gradient approximation made simple. *Phys. Rev. Lett.* **1996**, *77*, 3865. [[CrossRef](#)]
37. Andersen, H.C. Molecular dynamics simulations at constant pressure and/or temperature. *J. Chem. Phys.* **1980**, *72*, 2384–2393. [[CrossRef](#)]
38. Frisch, M.; Trucks, G.; Schlegel, H.; Scuseria, G.; Robb, M.; Cheeseman, J.; Scalmani, G.; Barone, V.; Petersson, G.; Nakatsuji, H. *Gaussian 16, Revision A. 03*; Gaussian, Inc.: Wallingford, CT, USA, 2016.
39. Zhao, Y.; Truhlar, D.G. A new local density functional for main-group thermochemistry, transition metal bonding, thermochemical kinetics, and noncovalent interactions. *J. Chem. Phys.* **2006**, *125*, 194101. [[CrossRef](#)] [[PubMed](#)]
40. Lu, T.; Chen, F. Multiwfns: A multifunctional wavefunction analyzer. *J. Comput. Chem.* **2012**, *33*, 580–592. [[CrossRef](#)] [[PubMed](#)]

41. Lu, T.; Chen, Q. Realization of Conceptual Density Functional Theory and Information-Theoretic Approach in Multiwfn Program. In *Conceptual Density Functional Theory: Towards a New Chemical Reactivity Theory*; Wiley: Hoboken, NJ, USA, 2022; Volume 2, pp. 631–647.
42. Yang, W.; Mortier, W.J. The use of global and local molecular parameters for the analysis of the gas-phase basicity of amines. *J. Am. Chem. Soc.* **1986**, *108*, 5708–5711. [\[CrossRef\]](#) [\[PubMed\]](#)
43. Humphrey, W.; Dalke, A.; Schulten, K. VMD: Visual molecular dynamics. *J. Mol. Graph.* **1996**, *14*, 33–38. [\[CrossRef\]](#)
44. Dennington, R.; Keith, T.A.; Millam, J.M. *GaussView 6.0. 16*; Semichem Inc.: Shawnee Mission, KS, USA, 2016; pp. 143–150.
45. Hafner, J.; Kresse, G. The vienna ab-initio simulation program VASP: An efficient and versatile tool for studying the structural, dynamic, and electronic properties of materials. In *Properties of Complex Inorganic Solids*; Springer: Berlin/Heidelberg, Germany, 1997; pp. 69–82.
46. Sun, J.; Ruzsinszky, A.; Perdew, J.P. Strongly constrained and appropriately normed semilocal density functional. *Phys. Rev. Lett.* **2015**, *115*, 036402. [\[CrossRef\]](#)
47. Fujinaga, T.; Watanabe, Y.; Shibuta, Y. Nucleation dynamics in Al solidification with Al-Ti refiners by molecular dynamics simulation. *Comput. Mater. Sci.* **2020**, *182*, 109763. [\[CrossRef\]](#)
48. Zhang, H.; Han, Y.; Dai, Y.; Lu, S.; Wang, J.; Zhang, J.; Shu, D.; Sun, B. An ab initio study on the electronic structures of the solid/liquid interface between TiB₂ (0 0 0 1) surface and Al melts. *J. Alloys Compd.* **2014**, *615*, 863–867. [\[CrossRef\]](#)
49. Domingo, L.R.; Ríos-Gutiérrez, M.; Pérez, P. Applications of the conceptual density functional theory indices to organic chemistry reactivity. *Molecules* **2016**, *21*, 748. [\[CrossRef\]](#) [\[PubMed\]](#)
50. De Vleeschouwer, F.; van Speybroeck, V.; Waroquier, M.; Geerlings, P.; de Proft, F. Electrophilicity and nucleophilicity index for radicals. *Org. Lett.* **2007**, *9*, 2721–2724. [\[CrossRef\]](#) [\[PubMed\]](#)
51. Chattaraj, P.K.; Maiti, B.; Sarkar, U. Philicity: A unified treatment of chemical reactivity and selectivity. *J. Phys. Chem. A* **2003**, *107*, 4973–4975. [\[CrossRef\]](#)
52. Oláh, J.; van Alsenoy, C.; Sannigrahi, A. Condensed Fukui functions derived from stockholder charges: Assessment of their performance as local reactivity descriptors. *J. Phys. Chem. A* **2002**, *106*, 3885–3890. [\[CrossRef\]](#)
53. Martínez-Araya, J.I. Why is the dual descriptor a more accurate local reactivity descriptor than Fukui functions? *J. Math. Chem.* **2015**, *53*, 451–465. [\[CrossRef\]](#)
54. Beck, M.E. Do Fukui function maxima relate to sites of metabolism? A critical case study. *J. Chem. Inf. Model.* **2005**, *45*, 273–282. [\[CrossRef\]](#) [\[PubMed\]](#)
55. Chattaraj, P.K.; Giri, S. Electrophilicity index within a conceptual DFT framework. *Annu. Rep. Sect. C Phys. Chem.* **2009**, *105*, 13–39. [\[CrossRef\]](#)
56. Chattaraj, P.K.; Roy, D.R. Update 1 of: Electrophilicity index. *Chem. Rev.* **2007**, *107*, PR46–PR74. [\[CrossRef\]](#)
57. Fuentealba, P.; Pérez, P. Contreras, On the condensed Fukui function. *J. Chem. Phys.* **2000**, *133*, 2544–2551. [\[CrossRef\]](#)
58. Han, Y.; Dai, Y.; Shu, D.; Wang, J.; Sun, B. First-principles calculations on the stability of Al/TiB₂ interface. *Appl. Phys. Lett.* **2006**, *89*, 144107. [\[CrossRef\]](#)
59. Edim, M.M.; Enudi, O.C.; Asuquo, B.B.; Louis, H.; Bisong, E.A.; Agwupuye, J.A.; Chioma, A.G.; Odey, J.O.; Joseph, I.; Bassey, F.I. Aromaticity indices, electronic structural properties, and fuzzy atomic space investigations of naphthalene and its aza-derivatives. *Heliyon* **2021**, *7*, e06138. [\[CrossRef\]](#) [\[PubMed\]](#)
60. Cao, J.; Ren, Q.; Chen, F.; Lu, T. Comparative study on the methods for predicting the reactive site of nucleophilic reaction. *Sci. China Chem.* **2015**, *58*, 1845–1852. [\[CrossRef\]](#)
61. Pino-Rios, R.; Inostroza, D.; Cárdenas-Jirón, G.; Tiznado, W. Orbital-weighted dual descriptor for the study of local reactivity of systems with (quasi-) degenerate states. *J. Phys. Chem. A* **2019**, *123*, 10556–10562. [\[CrossRef\]](#)
62. Fievez, T.; Sablon, N.; de Proft, F.; Ayers, P.W.; Geerlings, P. Calculation of Fukui functions without differentiating to the number of electrons. 3. Local Fukui function and dual descriptor. *J. Chem. Theory Comput.* **2008**, *4*, 1065–1072. [\[CrossRef\]](#)
63. Zhang, H.; Han, Y.; Dai, Y.; Wang, J.; Sun, B. An ab initio molecular dynamics study: Liquid-Al/solid-TiB₂ interfacial structure during heterogeneous nucleation. *J. Phys. D Appl. Phys.* **2012**, *45*, 455307. [\[CrossRef\]](#)

Disclaimer/Publisher’s Note: The statements, opinions and data contained in all publications are solely those of the individual author(s) and contributor(s) and not of MDPI and/or the editor(s). MDPI and/or the editor(s) disclaim responsibility for any injury to people or property resulting from any ideas, methods, instructions or products referred to in the content.